ECS Journal of Solid State Science and Technology, **3** (5) P143-P148 (2014)
2162-8769/2014/3(5)/P143/6/$31.00 © The Electrochemical Society

Electrochemical Oxidation as Vertical Structuring Tool for Ultrathin (d < 10 nm) Valve Metal Films

Kevin Stella,[a,d] Steffen Franzka,[a] Damian Bürstel,[a] Detlef Diesing,[a,*,z] Dirk Mayer,[b] and Vladimir Roddatis[c]

[a]*Fakultät für Chemie, Universität Duisburg-Essen, D-45117 Essen, Germany*
[b]*Peter Grünberg Institute, Jülich GmbH, 52425 Jülich, Germany*
[c]*CIC energiGUNE, 01510 Miñano, Álava, Spain*

Stepwise potentiostatic oxidation is used to reduce the thickness of thin aluminum and tantalum films from an initial thickness of 10 nm down to 2 nm. The thicknesses of the oxide and the residual metal are adjusted by the finite potential of an electrochemical oxidation procedure which consumes the initially 10 nm thick metal films. The metal–metal oxide interfaces are smooth and sharply defined. The metal consumption and oxide formation are proportional to each other by the ratio of their specific densities. This enables the derivation of a metal consumption factor for the residual metal film. Residual aluminum films show a significant increase of the specific resistivity with decreasing film thicknesses. This can be explained by modified electronic transport in the residual aluminum for example by changed electronic scattering processes at the metal–metal oxide interface or in the metal. Residual tantalum films show a weaker dependence of the specific resistivity down to 3 nm pointing to only slightly changed transport properties for electrons in the thin tantalum layers.

Manuscript submitted November 4, 2013; revised manuscript received February 27, 2014. Published March 15, 2014.

Heterojunctions as metal–insulator–metal (MIM) or metal–insulator–semiconductor junctions (MIS) junctions play a key role in electronic circuits. Thus, new routes to improve the properties or ease the preparation of these junctions are always of interest.[1-3] While gas phase oxidation[4] as well as plasma oxidation[5,6] are well established in device manufacturing, electrochemical techniques are rarely used. More often, electrochemical procedures are used in surface finishing with high temperatures and acid concentrations for fabrication of highly porous oxides. These porous oxide layers can be used as cover layer for the deposition of color pigments or as electrode surface with enlarged surface area.[7,8]

A less corrosive electrochemical method forming dense and electronically well-defined oxides was recently used for the preparation of so called chemoelectronic devices, which may be MIM[9,10] or MIS systems.[11] This method uses highly concentrated acetate electrolytes with a pH value of 6 and provides barrier type oxides. With these pH values the process of barrier formation is a factor of 1000 faster (typical oxide formation current density >100 $\mu A/cm^2$) than the process of corrosion (typical corrosion current density <0.1 $\mu A/cm^2$).[12] In this work we will show that this oxidation method can be used to prepare well defined metal–metal oxide sandwiches with adjustable metal thicknesses (d < 10 nm).

Miniaturization is not only a demand from electronic circuitry on the nanoscale. Since metal–metal oxide–metal sandwiches are also proposed for energy harvesting in chemical reactors,[13,14] there are also other reasons to minimize the thickness of each layer in a metal–metal oxide-metal sandwich.

There are three reasons, at least one for each layer:

- The top metal electrode serves as substrate for the catalytic reaction. When the reaction releases excited electrons the top electrode thickness should be lower than the mean free path of excited electronic carriers (usually <20 nm[15,16]).
- The intermediate oxide layer should not exceed 5 nm in thickness otherwise the transport of excited carriers through tunneling is inhibited.[17]
- The base metal layer should be as thin as possible to keep the overall device thickness small. This is important when the devices are expected to work as fast heat detectors. Then the device has a small heat capacity and even small energy fluxes can cause considerable temperature changes which can subsequently be clearly monitored by changes in the current voltage plots.[17,18]

An additional demand is the long-term stability of the oxide as well as of the underlying metal film. In a previous work, aging and degradation processes of electrochemically formed oxides were studied.[10] The conductivity of the underlying metal film was studied for 2 nm metal thickness and characteristic times for reaching an equilibrium state were found. This knowledge is used in the present work and the conductivity of the underlying metal film is measured always in the equilibrium state (after relaxation of the oxide), but for various thicknesses.

Of course it is questionable, whether a thickness value can be assigned to a partially consumed (oxidized) metal film. In case of a rough or cauliflower like interface structure the assignment of a thickness value to a partially consumed metal would be meaningless. Thus, cross sectional transmission electron microscopy is used to show the smoothness and sharp definition of the metal–metal oxide interface. Based on this result, assignment of a thickness and a newly introduced *film consumption factor* become meaningful. The metal film consumption factor allows a precise adjustment of metal thicknesses below 10 nm.

In the present work we apply electrochemical techniques for the production of metal–metal oxide structures where the thickness of the underlying metal film is scaled down to 2 nm. The two valve metals tantalum and aluminum are compared similar to our previous work.[10]

Thin aluminum films are known to grow polycrystalline. Due to the partial crystallinity the mean free path of conduction electrons is clearly higher than the thickness of 10 nm used in this work. Thus, multiple reflections of conduction electrons at the aluminum surface will influence the conduction and lead to quantum size effects in the thickness dependence of the film resistance, which are well known in aluminum,[19] as well as in coin metal films.[20]

Thin tantalum films prepared by e-beam evaporators exhibit an amorphous structure, the mean free path for electronic conduction in these films is significantly lower (4 Å see 21) than the thickness of 10 nm in this work.

Figure 1 shows the metal films in contact with an electrochemical droplet cell. Frequent scattering events in the tantalum film and mostly surface scattering events in the aluminum film are sketched. Reflections at the tantalum surface happen much more rarely than scattering events in the bulk. Quantum size effects in the thickness of the film resistance should then not appear. The specific resistivity of the tantalum films can be expected to be nearly independent on the film thickness.

*Electrochemical Society Active Member.
[d]Present address: Karlsruhe Institute of Technology, 76344 Eggenstein-Leopoldshafen, Germany.
[z]E-mail: detlef.diesing@uni-due.de

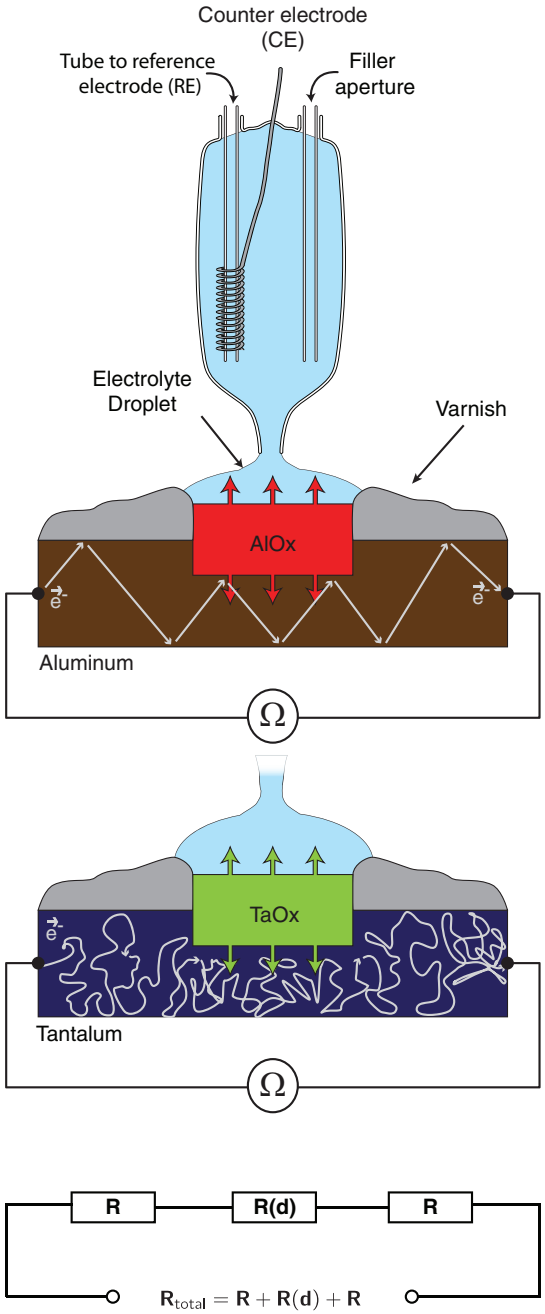

Figure 1. Schematic drawing of the samples and the electrical measurement set-up. The metal during oxide growth (shown as arrows) as well as possible electron pathways in the metals (mean free path in tantalum 4 Å, in aluminum several nm) are sketched. Bottom graph: serial circuit for analysis of $R(d)$.

Experimental

Preparation of the metal films.— The aluminum and tantalum films used in this work are 10 nm thick, 2 mm wide and 20 mm long. Aluminum films are evaporated from a thermal source containing a tungsten basket in a high vacuum chamber on microscope glass slides[4,9] whereas tantalum films are e-beam evaporated.[22] During deposition, the substrates are kept at room temperature. Slow deposition rates are chosen in both cases to ensure a good homogeneity of the metal films ([10,22]).

The evaporated metal films are studied via AFM. In figure 2 the topographies of the aluminum (left topography) and tantalum (right topography) films are shown for 10 nm thick samples. From these AFM-topographies one can exclude any overlaid structure on a 2 µm scale. However, especially from line scans, one can see that the aluminum film shows a quite high roughness (standard deviation in height $\sigma = \pm 1.4$ nm) whereas the tantalum film is quite smooth ($\sigma = \pm 0.2$ nm) which is consistent with our earlier results.[10,21,22]

Electrochemical anodic oxidation of films.— Metal films are thinned by an electrochemical oxidation procedure whereby a part of the metal is used to form metal oxide. This electrochemical oxidation is carried out in an electrolytic droplet cell,[9,23] see upper half of figure 1. A highly concentrated electrolyte is used ($c = 0.9$ mol/L). With this concentration the resistivity of the droplet cell is below 10 Ω. The potential drop in the electrolyte of the droplet cell is then negligible. Thus, the electrochemical potential difference applied between the metal film and the counter electrode drops solely at the metal–electrolyte interface leading to electrochemical surface reactions as oxidation. As salt the sodium salt of acetic acid is chosen. The organic anion has a low tendency to be incorporated during oxide growth. The resulting electrolyte acts also as buffer solution to minimize parallel corrosion processes like dissolving oxide during oxidation.[24]

A classical, waterproof, non conductive, varnish is used to define the oxidized area to 0.04 cm^2. After rinsing with MilliQ water and drying the samples in a nitrogen stream, the samples are transferred to an electrical resistance measurements unit described earlier[10] and sketched in figure 1, whereby we probe the resistance of the residual metal below the oxide. However, one has to note that this method is only applicable when the formed oxides are not conductive, as is the case here.[25,26]

The droplet is set on the metal surface when an initial potential of $E_{ini} = -1.2$ V is applied (with respect to SCE) between metal film and the counter electrode. Then a triangular potential ramp to the positive reverse potential E_{rev} and back to $E_{ini} = -1.2$ V is applied with a scan rate of 0,1 V / 2. In the first sweep E_{rev} is $+0.5$ V. $E_{rev.}$ is increased during the 18 sweeps to $+9.5$ V and the current voltage plots of surface oxidation (called cyclovoltammogram) are monitored, see figure 3.

For the oxidation the method of subsequent cyclovoltammograms is chosen since the aluminum films tend to stick on the glass substrate even when more than the half of the aluminum is oxidized. In comparative experiments with potential pulses (jumping directly from E_{ini} to E_{rev}) it was often observed that the aluminum films peel of from the glass substrate. Oxidation causes stress in the metal film.[27] Obviously, an oxidation in steps reduces the stress at the aluminum–glass interface. For tantalum there is no difference between a stepwise oxidation with subsequent cyclovoltammograms and a potential pulse to E_{rev}. The adherence of the tantalum films remains good, even if the film thickness is reduced by oxidation to more than 50%. In this respect oxidized tantalum films do not differ from pure tantalum films.[22] In this work the subsequent voltammetric oxidation is used for both metals.

The cyclovoltammograms show a typical passivation behavior. Once the oxide is formed for a specific value of E_{rev} the oxide cannot be reduced by simply applying any potential below E_{rev}. This means that current flow is negligible for voltages below the previously applied oxide formation voltage.

This can be seen for the whole series of experiments in figure 3. When the positive reverse potential of the cyclovoltammograms is increased from cycle to cycle, the oxidation current starts to flow just when the reverse potential of the former cyclovoltammogram is reached.

Between the 18 cyclovoltammograms the sample is carefully washed with deionized water and transferred to the electrical measurements unit where the resistance of the remaining metal film is measured. The aluminum and tantalum samples were treated in the same manner. The resulting cyclovoltammograms for aluminum look quite similar, hence are not shown here.

The flowed charge during the 18 different tantalum oxidation cyclovoltammograms (see figure 3) is integrated and plotted as function of positive return potential in figure 4. The summed charge of the

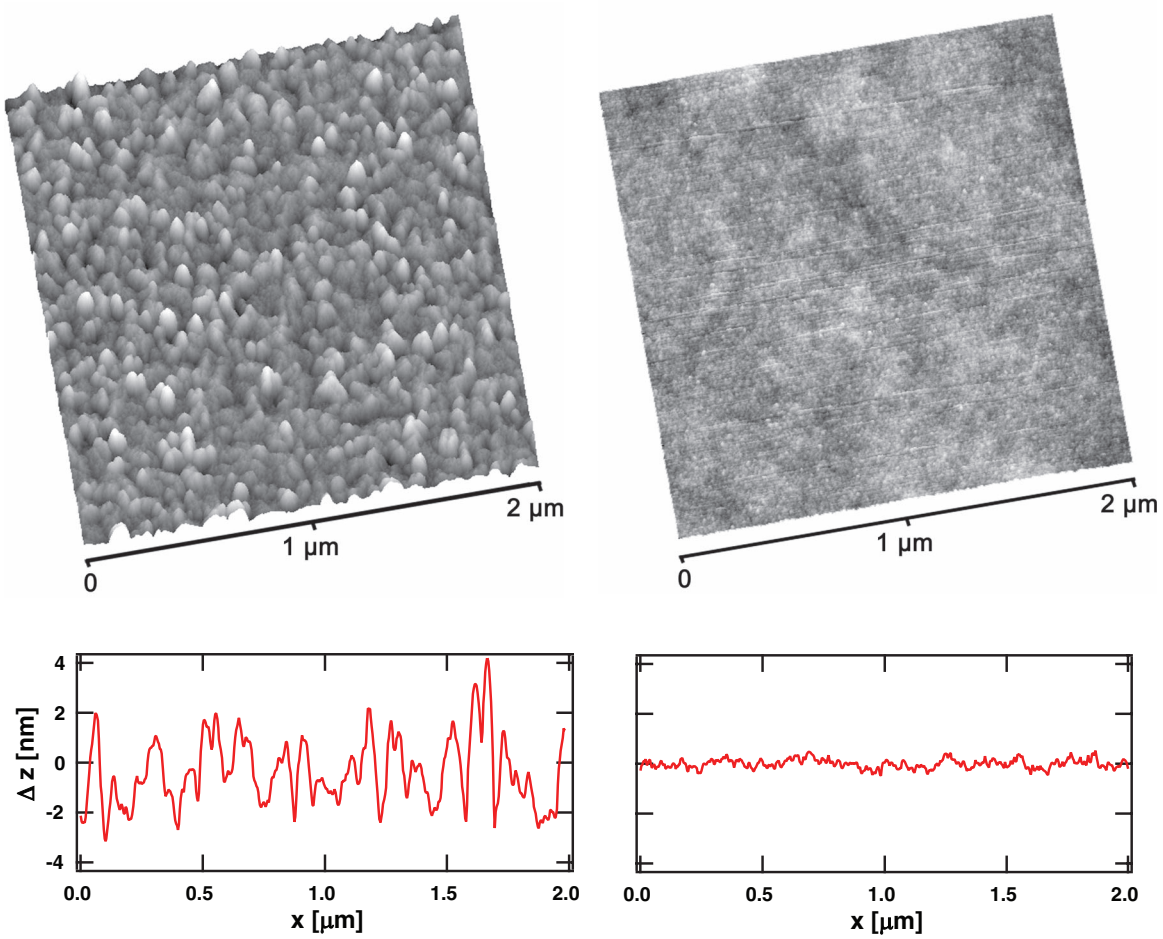

Figure 2. Left: Topography of aluminum film on glass with line scan shown below. **Right:** Topography of tantalum film on glass with line scan shown below.

subsequently carried out oxidations is plotted on the right y-axis versus the final oxidation potential in figure 4.

After the first cyclovoltammograms a nearly constant oxidation charge is measured. Therefore, the totally consumed charge during electrochemical oxidation of the tantalum shows a linear dependence on oxidation potential. When oxidizing with voltages $>$ 8.5 V (9 V and 9.5 V), one can clearly see a decrease in the flowed charge, see gray shaded area in figure 4. For other samples with thinner metal films one can observe a decrease in the flowed charge at lower voltages (not shown here). This means that less tantalum metal is oxidized and consumed to form the oxide. The most probable reason for this may be the increasing voltage drop in the residual metal for the last oxidations with thicker oxide.

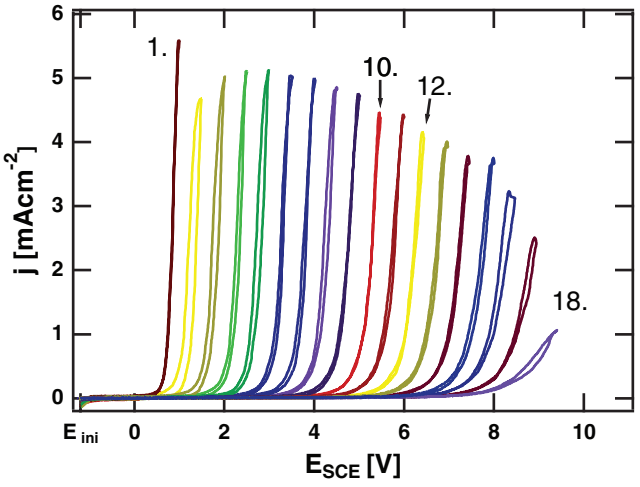

Figure 3. Subsequently carried out current-voltage plots (cyclovoltammograms) of the same tantalum sample with same initial potential $E_{ini} = -1.2$ V and 18 different positive reverse potentials. All potentials measured with respect to SCE (saturated calomel electrode).

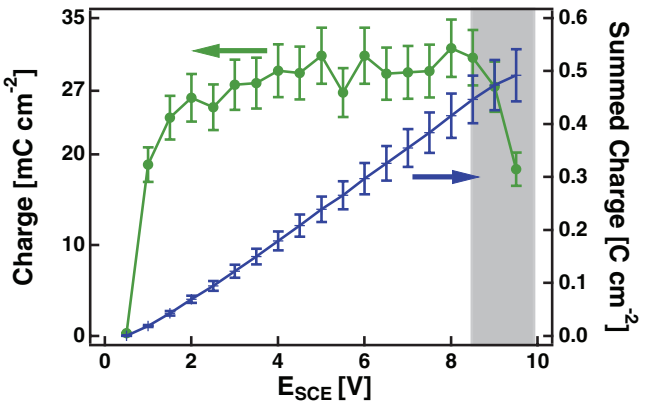

Figure 4. Left y axis: Flowed charge during the single cyclovoltammograms in figure 3 plotted versus the positive return potential. Right y axis: The summed charge of the subsequent cyclovoltammograms versus the positive return potential. Flowed charge during single cyclovoltammograms decrases due to the potential drop in the tantalum film for $E \geq 8.5$ V (gray shaded area).

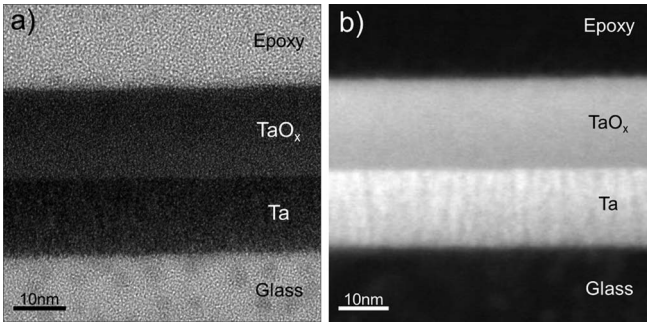

Figure 5. Bright field image (a) and dark field image (b) of a 20 nm thick tantalum film. Sharp Ta/TaOx and Ta/glass interfaces are clearly visible.

In the next step we want to estimate what fraction of the 10 nm thick metal films is consumed by oxidation cyclovoltammograms. Tantalum films with a 2 Volt oxide layer were transferred in an ultra high vacuum chamber and sputtered with a Gallium ion source. Among the sputter products, oxygen could be detected. The sample was sputtered for a definite time until the oxygen fraction in the sputter products decreased to less than the half. By a calibrated sputter yield a film formation factor of 2.1 nm/V was derived.[28] This is in a reasonable agreement with previous results (1.3 - 2.4 nm/V)[29,30] and agrees exactly with.[31] From these film formation factors one can estimate via the ratio of the densities of tantalum ($\rho_{Ta} = 16.6\,g/cm^3$)[32] and tantalum–oxide ($\rho_{Ta_2O_5} = 8.73\,g/cm^3$)[32] roughly a tantalum film consumption factor $r_{consum.}$(Ta) of $\approx 2.1\,(nm/V) \cdot (8.73/16.6) = 1.1\,nm/V$.

In a similar way one can derive an estimation for the aluminum film consumption factor $r_{consum.}$(Al). From an oxide film formation factor of 1.6-1.8 nm/V in the acetate electrolyte[4,33] (literature values in other electrolytes of 0.75 - 2 nm/V[29]) and the density ratio of the oxide ($\rho_{AlOx} = 3.95\,g\,cm^{-3}$)[34] and the metal (($\rho_{Al} = 2.7\,g\,cm^{-3}$))[35] one obtains a value of ≈ 1.2 nm/V for $r_{consum.}$(Al).

These estimated film consumption factors are crosschecked in the next section by cross sectional transmission electron microscope images.

Cross sectional TEM of oxidized tantalum samples.— Cross section specimens were prepared for **t**ransmission **e**lectron **m**icroscopy (TEM) study by the standard procedure that included mechanical polishing down to a thickness of 30 µm followed by ion milling (Ar^+) using Fischione 1010 Ion Mill (USA) at an accelerating voltage of 4 keV until the perforation. The study was performed using Tecnai F20ST (FEI, USA) electron microscope operating at an accelerating voltage of 200 kV. Dark-field images were recorded using high-angle annular dark-field detector (HAADF) for collecting electrons scattered through large angles.

For an easier preparation a 20 nm thick tantalum film sample with oxide layer formed at the applied reverse potential of 6 V was chosen as a specimen in the cross sectional TEM experiment. A cyclovoltammogram, like number 12 in figure 3 with a reverse potential of 6 V was used to prepare the oxide.

In figure 5 one can see a clear interface between tantalum and its oxide layer. The layer by layer oxidation suggested in figure 1 seems to be the dominating process during the consumption of the metal. In the dark field image one can easily estimate the thicknesses of the layers. The 20 nm thick tantalum film was consumed down to a thickness of 13 nm by an oxidation voltage of 6 V. This means a metal consumption factor of $r_{consum.}(Ta) = 7/6\,nm/V = 1.16\,nm/V$. This value coincides within some percent with the value of 1.1 nm/V derived in section II B. Hence, the metal film consumption factor derived by electrochemical methods is confirmed by microscopic techniques.

With the metal consumption factors one can then estimate the oxide's underlying metal film thickness. Subsequently it is possible to study the electrical resistivity as function of the metal film thickness by consuming the metal film.

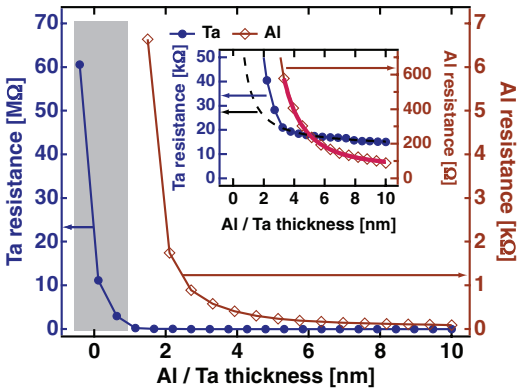

Figure 6. Electrical resistance of tantalum and aluminum films (underlying the oxide) versus metal film thickness. The questionable thickness values yielded by oxidation potentials $E \geq 8.5$ V are marked in a gray shaded box as in figure 4. The inset shows a zoom: The fit $R(d) \propto d^{-1}$ between 3.2 nm and 10 nm for the tantalum is marked as a black dashed line, whereas the power law fit $R(d) \propto d^{-2.4}$ for the aluminum resistance values is marked as solid red line.

Electrical resistivity of thin aluminum and tantalum films.— The electrical resistance of the specimen was measured by contacting the metal films with two interconnects consisting of conductive silver paste covering the whole width of the metal film. The initial resistance of the unoxidized 10 nm thick metal films covered with the non conductive varnish was 15000 Ω for tantalum and 98 Ω for aluminum (see inset in figure 6).

The resistance of the unoxidized samples was measured in the classical four point approach[20,36,37] as well as in the two terminal technique. Both methods coincided within 1% difference. This is not surprising since the resistance of the interconnects and the contact wires is much lower than the resistance of the sample. For the experiments with oxidized metal films the resistance of the specimen becomes even higher. Thus, the coincidence between the two and the four terminal method becomes even better and a four terminal method was not used for the experiments with electrochemically oxidized samples with oxidation potentials $E_{rev} > 1$ V.

Figure 6 shows the influence of the residual metal thickness on the metal films resistivity. The x-axis of the graph is yielded by setting

$$d(E) = 10\,nm - E \cdot r_{consum.}(Ta, Al). \quad [1]$$

Thickness values accomplished with high oxidation potentials > 8.5 V are shown in a gray box as in figure 4 since for these oxidation potentials $d(E) < 0.5$ nm. These unreasonable values show up due to the assumption that the metal consumption factor is valid up to high oxidation potentials. This is questionable since the cyclovoltammograms 15 till 18 in figure 3 show already a decrease in the flowed charge due potential drops in the residual tantalum film. Thus, nominal tantalum thicknesses inferred by oxidation potentials $E > 8.5$ V are disregarded for the further evaluation of the specific resistivity in figure 7.

To analyze the thickness dependence of the resistivity one has to keep in mind that the regions of the metal film which are covered by the varnish are not changed in thickness. Thus the data have to be analyzed as a series circuit of two constant and one variable resistor as shown in the lower part of figure 1. The resistivity of the tantalum film can be well described by a fit

$$R = R_0 + R(d) \quad , \quad R(d) \propto d^{-1} \quad [2]$$

for thicknesses between 3.2 and 10 nm. The fit is shown as black dashed line in the inset of figure 6. The proportionality between $R(d)$ and d^{-1} (similar to macroscopic samples) shows that scattering processes at the interfaces of the tantalum film do not play a role. This changes for $d < 3.2$ nm. Then the resistivity increases faster with decreasing thickness. This can be either attributed to starting

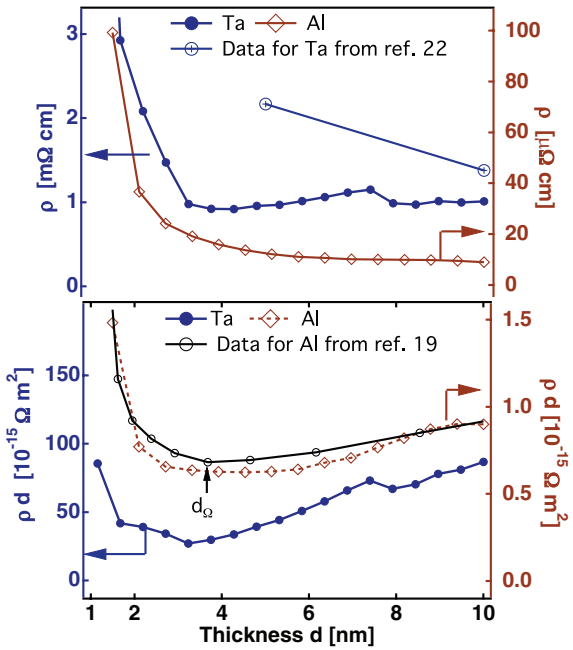

Figure 7. Upper graph: Specific resistivity ρ as a function of the film thickness d for tantalum and aluminum. **Lower graph:** Product of specific resistivity and film thickness $\rho \cdot d$ versus film thickness d. Additionally shown data for evaporated aluminum films are from figure 8 b) in reference 19.

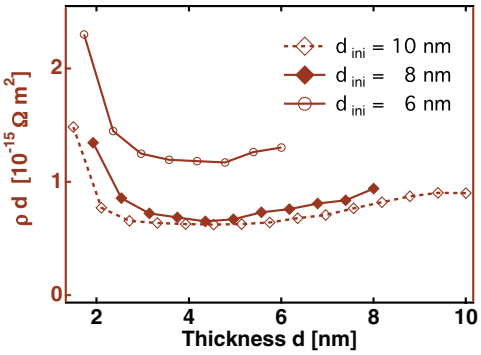

Figure 8. Product of specific resistivity and film thickness $\rho \cdot d$ versus film thickness d for aluminum films with different initial thicknesses.

contribution of interface scattering. Also one cannot exclude structure changes of the residual tantalum film as breaking coalescence[38] or increasing tensile stress changing the electron-phonon scattering.[39]

The thickness dependence of the aluminum films resistance cannot be described by the simple relationship $R(d) \propto d^{-1}$ over the whole thickness range. Instead the functional dependence of $R(d)$ on the thickness d is close to a power law with $R(d) \propto d^{-2.4}$ (added in the inset in figure 6 as a red curve). A power law like behavior is known to appear when mean free paths in the bulk are long and interface and surface scattering processes become dominant.[40,41]

The specific resistivity ρ of the the partially oxidized metal films can be evaluated by equations 1 and 2. ρ is shown as function of the thickness d in the upper graph of figure 7. The value for tantalum remains constant for thicknesses between 3.2 and 10 nm with a value of $\rho = 1\text{m}\Omega\text{cm} \pm 70\ \mu\Omega\text{cm}$. This value coincides partly with our previous results where the specific resistivity of freshly evaporated tantalum films was studied (figure 8 in 22). A value of 1.3 mΩcm was reported for a 10 nm thick film but a value of 2 mΩcm was found for a 5 nm thick film (see upper graph in figure 7). The big difference in the latter case is due to the limited validity of the evaluation for ρ in our setup. A part of the tantalum remains unoxidized under the varnish. Since the unoxidised tantalum has itself a quite high resistivity, a significant potential drop in these unoxidised areas will lead to an underestimation of the oxidized area's resistance. Thus, in the case for tantalum the specific resistivities during metal consumption have to be always critically compared with measurements using unoxidised films monitored during metal growth. However, the magnitude of the values for the specific resistivity is the same in growth and consumption experiments. For thicknesses $d < 3.2\,\text{nm}$ a sharp increase of ρ is observed which may be due to already discussed effects of breaking coalescence and tensile strain.

It should be mentioned that the specific resistivity for thin partially crystalline tantalum films is a factor of 3 − 5 lower for β − Ta.[42] However, sharp increases of for the specific resistivity with thinner tantalum films ($d < 7\,\text{nm}$) have also been observed for β − Ta.[43]

For aluminum, a monotonous increase of the specific resistivity can be observed (upper graph of figure 7) over the whole thickness range. In contrast to the amorphous tantalum one can expect for electronic conduction in s,p-electron dominated metals like the polycrystalline aluminum a mean free path larger than 10 nm. This means that scattering processes at the two surfaces of the metal determine the resistivity of the film.[44,45] The surface scattering dominated conduction leads in the nanometer range to finite size effects.[46,47] One parameter describing the surface scattering is the specularity parameter p. It is 1 for mirror like scattering and 0 for diffuse scattering. If the specularity parameter is independent on the film thickness the plot of $\rho \cdot d$ vs d should show a minimum value at the onset thickness of ohmic conduction (called d_Ω) and a linear increase for $d > d_\Omega$.[19]

Literature data for aluminum films grown in ultrahigh vacuum are shown in the lower graph of figure 7 (lower graph of figure 7, taken from figure 8(b) in reference 19). The resistivity was measured during film growth.[19] For these aluminum films the plot of $\rho \cdot d$ (data taken during film growth) shows a clear minimum d_Ω and a completely linear behavior for $d > d_\Omega$. For comparison, our data for the aluminum films during metal consumption (oxide growth) are shown. At first glance the data look quite similar. However, the minimum d_Ω is not so sharply defined for films consumed by oxidation as that for films growing in UHV. For $d > d_\Omega$ there is a small deviation from linearity for the films during consumption process. This points to a slightly changing interface roughness during the metal consumption process. However, the compliance of the literature data taken during metal growth and our data taken during metal consumption is very good meaning that the deviation between the two curves is only some percent and points to similar properties of the aluminum films.

A variation of the initial aluminum thickness (8 nm and 6 nm in figure 8) shows a comparable behavior with a minimum value d_Ω for $\rho \cdot d$. It was observed that the $\rho \cdot d$ values for aluminum films with $d_{ini} = 6\,nm$ were always higher than for thicker films. The values for a typical sample are shown in figure 8. The reason might be that our manual varnishing technique under a magnifying glass always harms the metal film a bit. This harming effect can be more effective for thinner films than for thicker ones. However the influence of the electrode potential and the thinning of the metal film is comparable for different initial metal thicknesses d_{ini}.

Conclusion.— A new approach for the joint fabrication of nanoscaled metal films and metal oxide films was shown. The vertical structuring process uses localized electrochemical anodic oxidation for ultrathin valve metal films.

Therefore thin aluminum and tantalum films structured by electrochemical anodic oxidation were studied using the in situ electrochemical current response, TEM, AFM, and thickness dependent resistivity. For the first time, systematic studies on the thickness dependence of a metal film resistance are performed by metal consumption experiments. Therefore anodic oxidation was carried out to enable an easy preparation of very thin metal layer thicknesses. A linear response of the metal consumption to the applied electrochemical oxidation potential was observed. In addition to the established oxide formation factors for the metals tantalum and aluminum, a metal consumption

Table I. Comparison of oxide formation factors (literature and this work) and metal consumption factors revealed in this work.

	Oxide formation factor	Metal consumption factor
Ta	2.1 nm/V[29–31]	1.1 nm/V
Al	1.6 − 1.8 nm/V[4,33]	1.2 nm/V

factor could be derived. The metal consumption factor is proportional to the oxide formation factor. The proportionality factor can be well estimated by the ratio of specific densities of metal to its oxide for aluminum and tantalum see table I.

With the proper choice of electrolyte and oxidation potential, the electrochemical oxidation combined with droplet cells can work like a molding cutter on nanoscale dimensions. Furthermore it is shown that electrochemical processes are suitable at room temperature and neutral pH-value to form sharply defined and very smooth metal-metal–oxide interfaces. The future will show where the main interest fields for this new method will lie. We believe that it will shed new light on electrochemically structured films and valve metal studies.

Acknowledgment

This work is supported by the Deutsche Forschungsgemeinschaft in the frame of the SFB 616 “Energy Dissipation Processes at Surfaces”. K. S. wishes to thank the “Studienstiftung des deutschen Volkes” for support. The authors want to thank Katrin Astemann and Achim W. Hassel for various discussions. Proof reading by Ievgenii Nedrygailov and Nitha Enasu is gratefully acknowledged.

References

1. S. Grover, O. Dmitriyeva, M. J. Estes, and G. Moddel, *Nanotechnology, IEEE Transactions on*, **9**, 716 (Nov. 2010).
2. D. Connelly, C. Faulkner, D. E. Grupp, and J. S. Harris, *Nanotechnology, IEEE Transactions on*, **3**, 98 (March 2004).
3. M. Y. Doghish and F. D. Ho, *Electron Devices, IEEE Transactions on*, **39**, 2771 (1992).
4. D. Diesing, A. W. Hassel, and M. M. Lohrengel, *Thin Solid Films*, **342**, 282 (1999).
5. E. Cimpoiasu, S. K. Tolpygo, X. Liu, N. Simonian, J. E. Lukens, K. K. Likharev, R. F. Klie, and Y. Zhu, *Journal of Applied Physics*, **96**, 1088 (2004).
6. P. Rottländer, M. Hehn, O. Lenoble, and A. Schuhl, *Appl. Phys. Lett.*, **78**, 3274 (2001).
7. S. Tan, M. Reed, H. Han, and R. Boudreau, *Micro Electro Mechanical Systems, 1995, MEMS '95, Proceedings. IEEE* pp. 267 (1995).
8. O. Rabin, P. R. Herz, Y. M. Lin, A. I. Akinwande, S. B. Cronin, and M. S. Dresselhaus, *Advanced Functional Materials*, **13**, 631 (2003).
9. Y. Jeliazova, M. Kayser, B. Mildner, A. W. Hassel, and D. Diesing, *Thin Solid Films*, **500**, 330 (2006).
10. K. Stella and D. Diesing, *Journal of The Electrochemical Society*, **154**, C663 (2007).
11. K. Stella, D. A. Kovacs, and D. Diesing, *Electrochemical and Solid-State Letters*, **12**, H453 (2009).
12. J. Schulze and A. W. Hassel, Passivity of metals, alloys and semiconductors (Wiley VCH, Weinheim, 2003), vol. 4 of *Encyclopedia of Electrochemistry*, chap. 3.2, p. 216.
13. A. Hervier, J. R. Renzas, J. Y. Park, and G. A. Somorjai, *Nano Letters*, **9**, 3930 (2009).
14. J.Y. Park and G. Somorjai, *ChemPhysChem*, **7**, 1409 (2006).
15. B. Mildner, E. Hasselbrink, and D. Diesing, *Chemical Physics Letters*, **432**, 133 (2006).
16. H. Nienhaus, *Surf. Sci. Rep.*, **45**, 1 (2002).
17. D. Diesing, D. Kovacs, K. Stella, and C. Heuser, *Nuclear Instruments and Methods in Physics Research Section B: Beam Interactions with Materials and Atoms*, **269**, 1185 (2011).
18. I. I. Nedrygailov, E. G. Karpov, E. Hasselbrink, and D. Diesing, *Journal of Vacuum Science & Technology A: Vacuum, Surfaces, and Films*, **31**, 021101 (2013).
19. H. Hoffmann and J. Vancea, *Thin Solid Films*, **85**, 147 (1981).
20. H. D. Liu, Y. P. Zhao, G. Ramanath, S. P. Murarka, and G. C. Wang, *Thin Solid Films*, **384**, 151 (2001).
21. K. Stella, D. Bürstel, E. Hasselbrink, and D. Diesing, *physica status solidi (RRL) – Rapid Research Letters*, **5**, 68 (2011).
22. K. Stella, D. Bürstel, S. Franzka, O. Posth, and D. Diesing, *Journal of Physics D: Applied Physics*, **42**, 135417 (2009).
23. A. W. Hassel and M. M. Lohrengel, *Electrochim. Acta*, **42**, 3327 (1997).
24. A. W. Hassel and M. M. Lohrengel, *Electrochim. Acta*, **40**, 433 (1995).
25. V. Macagno and J. W. Schultze, *Journal of Electroanalytical Chemistry*, **180**, 157 (1984).
26. K. Stella, D. A. Kovacs, D. Diesing, W. Brezna, and J. Smoliner, *Journal of The Electrochemical Society*, **158**, P65 (2011).
27. J. C. Nelson and R. A. Oriani, *Corrosion Science*, **34**, 307 (1993).
28. K. Asteman, A. Hassel, K. Stella, D. Diesing, and A. Mardare, in preparation.
29. J. W. Schultze and M. M. Lohrengel, *Electrochimica Acta*, **45**, 2499 (2000).
30. A. Mardare, A. Ludwig, Alan Savan, and Achim Walter Hassel, *Science and Technology of Advanced Materials*, **15**, 015006 (2014).
31. F. Di Franco, G. Zampardi, M. Santamaria, F. Di Quarto, and H. Habazaki, *Journal of The Electrochemical Society*, **159**, C33 (2011).
32. K. Andersson, K. Reichert, and R. Wolf, Tantalum and Tantalum Compounds (*Ullmann's Encyclopedia of Industrial Chemistry*, Wiley VCH, 2000), p. 10.
33. A. W. Hassel and D. Diesing, *Thin Solid Films*, **414**, 296 (2002).
34. M. Chmielewski and K. Pietrzak, *Journal of the European Ceramic Society*, **27**, 1273 (2007).
35. M. A. Rabah, *Waste Management*, **23**, 173 (2003).
36. B. J. Horkstra, L. J. Van Der Pauw, and N. V. Philips, *Journal of Electronics and Control*, **7**, 169 (1959).
37. M. Li and G.-C. Wang, *Review of Scientific Instruments*, **69**, 1811 (1998).
38. W. Nix and B. Clemens, *Journal of Materials Research*, **14**, 3467 (1999).
39. R. Abermann and R. Koch, *Thin Solid Films*, **129**, 71 (1985).
40. P. Wissmann, Thin metal films and gas chemisorption, *Studies in surface science and catalysis*; 32 (Elsevier, Amsterdam, 1987).
41. C. Kunze, *Solid State Communications*, **87**, 359 (1993).
42. K. Ino, T. Shinohara, T. Ushiki, and T. Ohmi, *Journal of Vacuum Science & Technology A: Vacuum, Surfaces, and Films*, **15**, 2627 (1997).
43. O. A. Novodvorsky, O. D. Khramova, C. Wenzel, and J. W. Bartha, *Technical Physcis*, **50**, 715 (2005).
44. D. Schumacher, *Thin Solid Films*, **151**, 499 (1987).
45. G. Kästle, H.-G. Boyen, A. Schröder, A. Plettl, and P. Ziemann, *Physical Review B*, **70**, 165414 (2004).
46. E. H. Sondheimer, *Advances in Physics*, **1**, 1 (1952).
47. F. Sajovec, P. M. Meuffels, and T. Schober, *Thin Solid Films*, **219**, 206 (1992).